PROCEEDINGS OF SPIE

SPIEDigitalLibrary.org/conference-proceedings-of-spie

Resonance properties of isolatedparticle optical lattices: Antireflectionquenched Mie scattering and Mie modal memory

Robert Magnusson, Yeong Hwan Ko, Nasrin Razmjooei, Fairooz Abdullah Simlan, Hafez Hemmati

Robert Magnusson, Yeong Hwan Ko, Nasrin Razmjooei, Fairooz Abdullah Simlan, Hafez Hemmati, "Resonance properties of isolated-particle optical lattices: Antireflection-quenched Mie scattering and Mie modal memory," Proc. SPIE 12010, Photonic and Phononic Properties of Engineered Nanostructures XII, 1201002 (5 March 2022); doi: 10.1117/12.2607963



Event: SPIE OPTO, 2022, San Francisco, California, United States

Resonance properties of isolated-particle optical lattices: Antireflection-quenched Mie scattering and Mie modal memory

Robert Magnusson, Yeong Hwan Ko, Nasrin Razmjooei, Fairooz Abdullah Simlan, Hafez Hemmati Department of Electrical Engineering, University of Texas Arlington, Arlington, Texas 76019, USA

ABSTRACT

Periodic optical lattices consisting of isolated-particle arrays in vacuum are treated with rigorous electromagnetics. These structures possess a wealth of interesting properties including perfect reflection across small or large spectral bandwidths depending on the choice of materials and design parameters. Pertinent spectral expressions have been observed theoretically and experimentally via one-dimensional (1D) and two-dimensional (2D) structures commonly known as resonant gratings, metamaterials, and metasurfaces. The physical cause of perfect reflection and related properties is guided-mode resonance mediated by lateral Bloch modes excited by evanescent diffraction orders in the subwavelength regime. Here, we review recent results on differentiation of local Mie resonance and guided-mode lattice resonance in causing resonant reflection by periodic particle assemblies. We treat a classic 2D periodic array consisting of dielectric spheres. To disable Mie resonance, we apply antireflection (AR) coatings to the spheres. Reflectance maps for coated and uncoated spheres demonstrate that perfect reflection persists in both cases. We find that the Mie scattering efficiency of an AR-coated sphere is greatly diminished. Additionally, in a 1D cylindrical rod-type lattice, we investigate and compare local field profiles in periodic assemblies and in the constituent isolated particles. In general, the lattice and particle resonance wavelengths differ. When the lateral leaky-mode field profiles approach the isolated-particle Mie field profiles, the resonance locus tends towards the Mie resonance wavelength. This correspondence is referred to as Mie modal memory. These fundamentals may help distinguish Mie effects and leaky-mode lattice effects in generating the observed spectra in this class of optical devices while elucidating the basic resonance properties across the entire spectral domain.

Keywords: guided-mode resonance effect, leaky-mode resonance, resonant waveguide gratings, metamaterials, Bloch modes, Mie scattering, leaky-band dynamics, Mie modal memory, metasurfaces

1. INTRODUCTION

Resonant optical lattices can be configured with periodic assemblies of arbitrarily shaped particles. The particles may be in the form of pillars, blocks, or rods composed of metals, dielectrics, or semiconductors. Optical lattices are, in general, three-dimensional (3D) as are their crystalline counterparts. However, important variants in the form of 2D or 1D patterned films or membranes exist in the optical domain. The isolated-particle optical lattices in focus here refer to particle arrays residing in vacuum for analytical and physical simplicity. Although the fundamental periodic element, namely the diffraction grating, has been known for more than 100 years, new solutions and applications based on spatially periodic modulations continue to appear. In recent literature, corresponding assemblies and devices are called metamaterials or metasurfaces and the like. Current lithographic technology enables fabrication of spatial modulations on subwavelength scales in one, two, or three dimensions even at visible or UV wavelengths. The resulting diffractive optical elements (DOE) or metasurfaces may support waveguide modes if the refractive indices and dimensions of the element are correctly chosen; these devices are often termed waveguide gratings in past literature. Waveguide modes that are guided or quasi-guided in waveguide gratings experience stopbands and passbands as the light frequency is varied. Nano- and microstructured lattices with subwavelength periodicity support guided-mode resonance effects and therefore represent fundamental building blocks for a host of device concepts on account of the diversity of spectral expressions mediated by the resonance effect. For many real-world applications, 1D and 2D photonic lattices exhibit attractive features such as compactness, minimal interface count, high efficiency, and potential monolithic fabrication with attendant robustness under harsh conditions. The governing resonance effects hold across the spectrum, from visible wavelengths to the microwave domain, by simple scaling of wavelength to period and proper materials specification. Background on the physics, formulation, experiments, characterization, and applications of resonant photonic elements can be found in selected references [1-21]. Some of these references are from our group as we have studied this field of research and technology theoretically and experimentally for more than 30 years.

*magnusson@uta.edu; phone 1 817 272-2672; fax 1 817 272-2253; www.leakymoderesonance.com

Photonic and Phononic Properties of Engineered Nanostructures XII, edited by Ali Adibi, Shawn-Yu Lin, Axel Scherer, Proc. of SPIE Vol. 12010, 1201002 © 2022 SPIE · 0277-786X · doi: 10.1117/12.2607963

If the particles in the array are positioned randomly, the assembly scatters incident light incoherently with random phasing thereby losing all major properties including perfect reflection and generation of discrete propagating and evanescent diffraction orders. The individual particles will resonate light in a local manner with scattering amplitudes and directional properties depending on materials, particle shape, and proximity to neighboring particles. Fabry-Perot (FP) resonance occurs via reflections between parallel planes possessing refractive-index discontinuities and is typically associated with thin films. Mie resonance occurs by similar reflections but between nonparallel planes and is generally associated with isolated cylindrical and spherical particles [22]. Mie resonance can be considered a generalized FP resonance in arbitrary geometries. In strictly periodic lattices, the incident light develops a spatially periodic phase creating diffracted waves propagating in directions depending on the wavelength as expressed in the grating equation. This underlies the spectroscopic properties of diffraction gratings. An entire field of technology, namely diffractive optics, addresses attendant theory, design, fabrication, and applications. Diffractive optical elements affect the spatial distribution, spectral content, energy content, polarization state, and propagation direction of an optical wave. Common applications include spectral filters, diffractive lenses, antireflection surfaces, beam splitters, beam steering elements, laser mirrors, polarization devices, beam-shaping elements, couplers, and switches. These components are widely used in lasers, fiber-optic communication systems, spectroscopy, medical technology, integrated optics, imaging, and in many other optical systems.

In this paper, we review recent results espousing the physical principles of resonant leaky-mode lattices. We address differentiation of Mie resonance and guided-mode resonance in mediating resonant reflection by periodic particle assemblies. We treat a classic 2D periodic array consisting of silicon spheres. To disable Mie resonance, we apply an optimal antireflection (AR) coating to the spheres. Reflectance maps for coated and uncoated spheres demonstrate that perfect reflection persists in both cases. Additionally, in a 1D cylindrical rod-type lattice, we compare local field profiles in periodic assemblies and in the constituent isolated particles. When the lateral leaky-mode field profiles approach the isolated-particle Mie field profiles, the resonance locus tends towards the Mie resonance wavelength. This convergence is referred to as Mie modal memory. A fuller description is provided in the papers reviewed here [23, 24].

2. RESONANCE PROPERTIES OF ARRAYS OF UNCOATED NANOSPHERES

We model a periodic array composed of nanospheres where n and D denote refractive index and diameter as illustrated in Fig. 1(a). The particles are arrayed in a 2D lattice with period Λ embedded in air or vacuum with refractive index $n_{air} = 1$. The input beam is modeled as a plane wave at normal incidence with fixed polarization (electric-field vector along the y-axis while the magnetic field points along the x-axis).

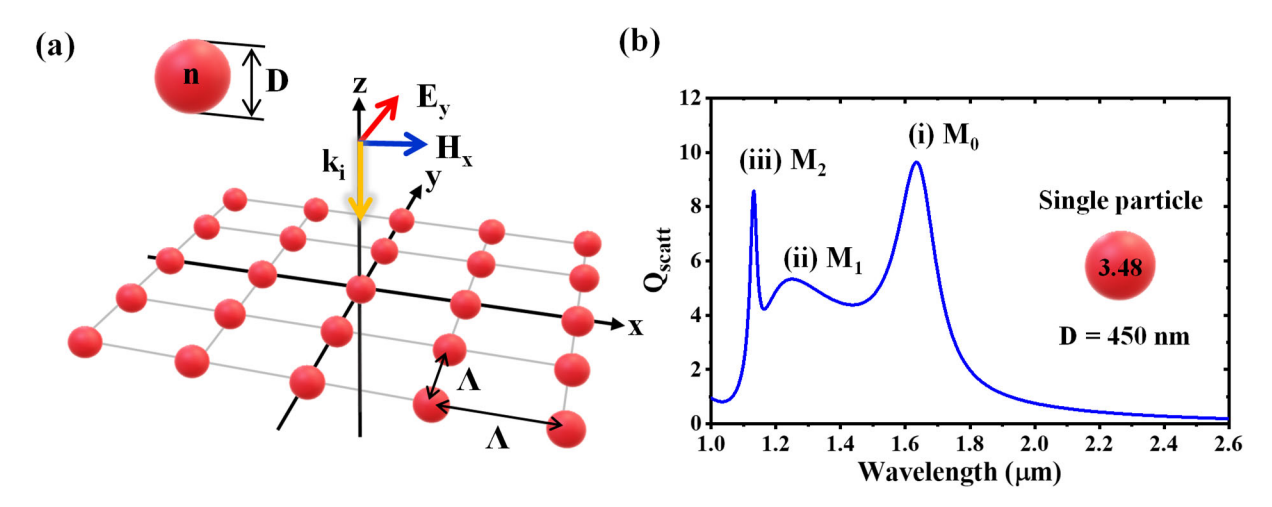


Figure 1. (a) Schematic of a 2D photonic lattice composed of nanospheres where n and D label refractive index and diameter of the sphere. Each nanosphere is arranged by the lattice period ($\Lambda = \Lambda_x = \Lambda_y$). The input is a plane wave at normal incidence with its electric-field vector along the y-axis while the magnetic-field vector is along the x-axis. (b) Total scattering efficiency (Q_{scatt}) spectrum of a single Si sphere (n= 3.48, D= 450 nm). At (i) λ =1.634 μ m (M_0), (ii) λ =1.25 μ m (M_1) and (iii) λ =1.13 μ m (M_2), Mie resonances appear identified as classic magnetic dipole, electric dipole, and magnetic quadrupole response, respectively [24].

Figure 1(b) shows the total scattering efficiency (Q_{scatt}) of an isolated silicon sphere with a fixed, nondispersed refractive index n = 3.48 and diameter D = 450 nm. It is calculated using analytical formulas from Mie scattering theory as [25]

$$Q_{scatt} = \frac{2}{\alpha^2} \sum_{n=1}^{\infty} (2n+1)(|a_n|^2 + |b_n|^2)$$
 (1)

In this expression, $\alpha = \pi D/\lambda$ is the size parameter with λ being the wavelength in free space and a_n and b_n are the Mie scattering coefficients. In the spectrum, familiar Mie resonances appear at (i) $\lambda = 1.634 \,\mu\text{m}$ (M₀), (ii) $\lambda = 1.25 \,\mu\text{m}$ (M₁) and (iii) $\lambda = 1.13 \,\mu\text{m}$ (M₂) which are contributed by the magnetic dipole, electric dipole, and magnetic quadrupole, respectively.

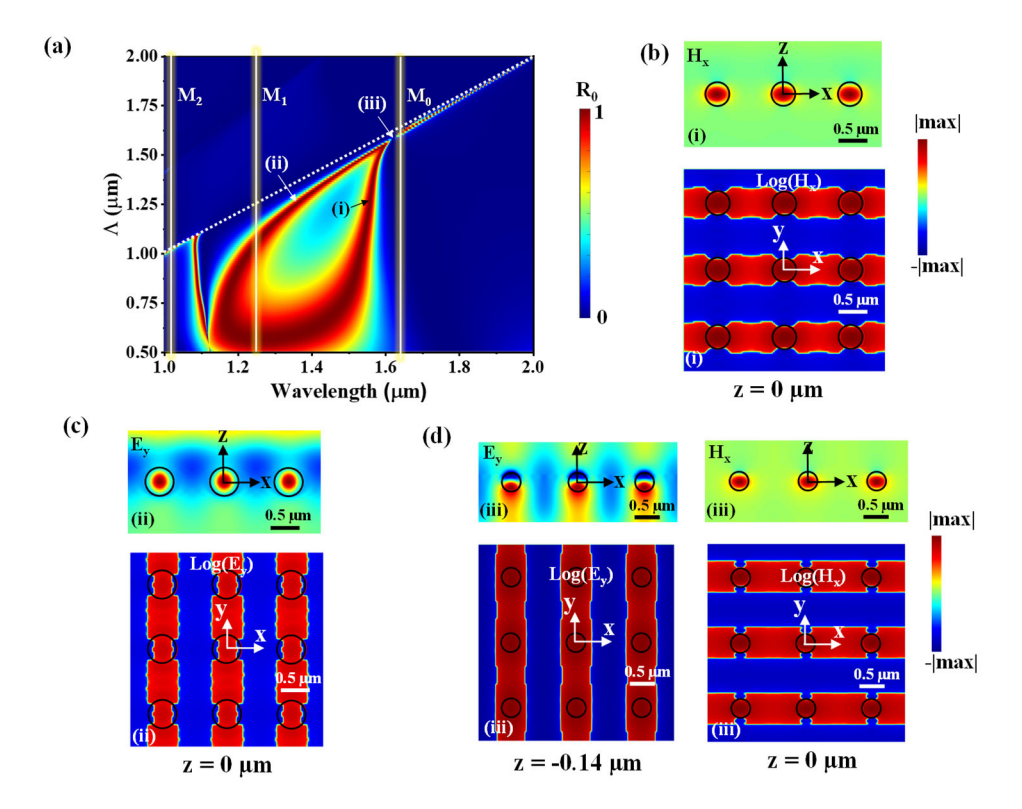


Figure 2. Perfect reflection bands generated by a resonant photonic lattice. (a) Calculated R_0 spectral map as a function of Λ . For comparison, Mie resonance locations (M_0 - M_2) are displayed by vertical lines. The white dashed line indicates the Rayleigh line (Λ = λ). (b)-(d) Representative E and H profiles associated with the photonic lattice at (i) Λ = 1.25 μ m, λ = 1.522 μ m, (ii) Λ = 1.25 μ m, λ = 1.372 μ m and (iii) Λ = 1.58 μ m, λ = 1.62 μ m. Shown are localized fields at the nanospheres on a linear scale (upper plots) as well as standing wave interference patterns of lateral counter-propagating Bloch modes on a log scale (lower plots) at these points as marked in (a). Point (i) and fields in (b) pertain to TM0 modes propagating along \pm y. Point (ii) and fields in (c) correspond to TE0 modes propagating along \pm x. Point (iii) locates in the reflection null on the merged mode line where these TM0 and TE0 modes overlap. The fields in (d) correspond to this point. The lateral Bloch modes exhibit standing waves along the x direction (TE mode) and y direction (TM mode). These modes travelling along orthogonal directions are copolarized for the excitation shown in Fig. 1 and thus the reflected waves due to each mode can interfere effectively to cancel the reflection and to yield perfect transmission at that point as shown in the spectrum. We note that the local fields in (d) are those of the overlapping TE0 and TM0 modes and cannot represent these modes individually. The log-scale amplification of the standing waves makes them look artificially sharp [24].

We calculate reflectance spectra of this photonic lattice versus Λ by performing rigorous coupled-wave analysis [26, 27]. When this lattice is in the subwavelength regime, only zero-order reflectance (R_0) remains, and perfect reflection is possible. Figure 2(a) shows the R_0 color map as a function of Λ from 0.5 to 2 μ m. For comparison, the wavelengths corresponding to M_0 , M_1 and M_2 are also indicated by vertical lines. The perfect reflection loci (displayed in dark red color) are controlled by the period of the lattice. This is because the period strongly affects the homogenized effective-medium refractive index of the lattice which, in turn, defines the character and properties of the lateral leaky Bloch modes.

As Λ increases, the reflection band changes in resonance wavelength position up to the Rayleigh line (Λ = λ , displayed by a white dashed line). Beyond the Rayleigh line, $R_0 < 1$ because higher propagating diffraction orders draw power. For points (λ , Λ) under the Rayleigh line, subwavelength conditions prevail and no higher-order diffracted waves propagate. We note that the Mie lines are not correlated directly with the reflection band. Figures 2(b)-(d) provide representative electric (E) and magnetic (H) field profiles associated with the photonic lattice at (i) Λ = 1.25 μ m, λ = 1.522 μ m, (ii) Λ = 1.25 μ m, λ = 1.372 μ m and (iii) Λ = 1.58 μ m, λ = 1.62 μ m. These panels illustrate the localized fields at the nanospheres on a linear scale (upper plots) as well as the standing-wave interference patterns of the lateral counter-propagating Bloch modes on a log scale (lower plots) at these points as marked in Fig. 2(a). Point (i) and fields in Fig. 2(b) pertain to TM₀ modes propagating along \pm y. Point (ii) and the fields in Fig. 2(c) correspond to TE₀ modes propagating along \pm x. Point (iii) locates in the reflection null on the merged mode line where the TM₀ and TE₀ modes overlap. The fields in Fig. 2(d) correspond to this point. The coexisting Bloch modes exhibit standing waves along the x direction (TE mode) and y direction (TM mode). These modes travelling along orthogonal directions are copolarized for the excitation field shown in Fig. 1 that has an electric-field vector along the y direction. Therefore, the reflected waves due to each mode can interfere effectively to cancel the reflected wave and to yield perfect transmission at that point as shown in the spectrum.

3. RESONANCE PROPERTIES OF ARRAYS OF AR-COATED NANOSPHERES

Figure 3 indicates that Mie scattering resonance is subdued by the AR effect where the AR film thickness (d =220 nm) is chosen for the wavelength of M₀ (λ =1.634 µm) of the original Si sphere. Viewing the computed results in Fig. 3, the localized signature is greatly diminished relative to the strongly confined fields in the uncoated sphere as in Fig. 1(b). There is still heightened concentration in the center of the sphere relative to background because it is impossible to perfectly cloak it with a single AR film. Owing to the AR effect and attendant low backward scattering, much of the light passes through the particle with dominant forward scattering. In addition, as seen in the TSCS spectrum of Fig. 3(c), the two resonance peaks from Fig. 1(b) are significantly broadened and the total scattering efficiency is reduced. Relative to the M₀ position of the original uncoated Si sphere, the Mie scattering resonance is red-shifted and the quality (Q) factor of the resonance decreases. Figure 4(d) illustrates the local field structure at the wavelength of M₀ (λ =1.634 µm).

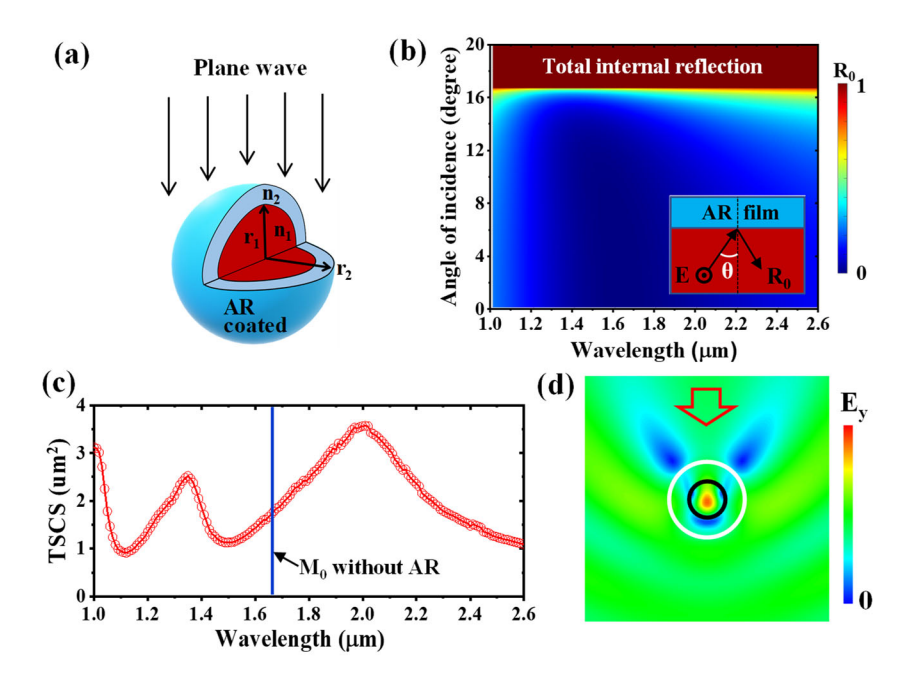


Figure 3. Effects of AR coating on the scattering properties of the nanosphere with AR-film thickness d=220 nm. (a) AR-coated sphere model. (b) Schematic of total internal reflection for the curved geometry. (c) TSCS spectra of the coated sphere. (d) Electric field profile corresponding to the Mie resonance peak at the M_0 wavelength.

Finally, we demonstrate perfect reflection with the AR-coated Si spheres in the photonic lattice. Thus, Fig. 4(a) shows a calculated R_0 (λ , Λ) map for a 2D array of spheres. Perfect reflection bands appear in the spectral region displayed contributed by lattice-generated GMR. As can be seen in the field profiles of Fig. 4(b), standing wave patterns form due to interference between counterpropagating lateral Bloch modes. Lattice resonance induces strong optical confinement even if the local cavity of each individual particle is eliminated. This is because the lattice, in spite of the AR coat on the particles, still exhibits finite values of effective refractive index on which to support the modes. The AR-coat design wavelength is 1.634 μ m with efficient reflection occurring near this wavelength irrespective of the AR coat.

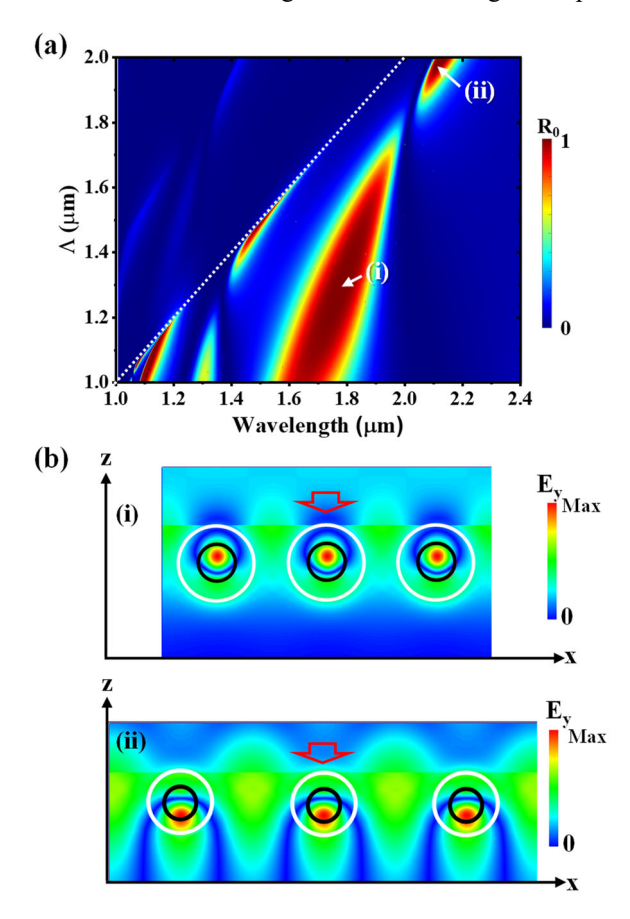


Figure 4. Perfect reflection bands generated by a 2D resonant photonic lattice built with AR-coated Si spheres. (a) $R_0(\lambda, \Lambda)$ map. (b) Field profiles at points (i) and (ii).

4. DIFFERENTIATION OF MIE RESONANCE AND LATTICE RESONANCE

Figure 5 illustrates models and spectra pertaining to Mie resonance in isolated particles and guided-mode resonance in periodic lattices. For this example, the model particle chosen is an infinite circular cylinder with diameter D and refractive index n placed in air (Fig. 5a). The lattice is an array of similar particles with period Λ (Fig. 5d). The lattice operates in the subwavelength regime such that only the zero-order reflectance (R_0) and zero-order transmittance (T_0) are shown in Fig. 5(d). The illuminating plane wave is at normal incidence with wavenumber k_i . As usual in diffraction and waveguide optics, we define TE and TM polarization state as electric field parallel and perpendicular to the particle axis. Figure 5(b) presents the total scattering cross section (TSCS) of a single particle with D = 250 nm and refractive index n = 2. Similarly, Fig. 5(c) provides the TCSC for n=3.5. On account of the cylinder geometry, we label the Mie resonance field configuration in terms of azimuthal mode number (j) and radial mode number (l) as $TE_M(j, l)$ or $TM_M(j, l)$ [28]. In Fig. 1(c), $TE_M(1, 1)$ and $TM_M(0, 1)$ are located at $\lambda = 1.179$ µm and 1.173 µm, respectively, or close to each other. Obviously, the TE-polarized TSCS exceeds the TM-polarized TSCS because TM light encounters Brewster conditions at the cylinder surface resulting

in lower TM reflection and less effective scattering. Figure 5(e) presents R_0 spectra under TE and TM polarization for n=2. The resonance peaks are labeled $TE_L(m, v)$ or $TM_L(m, v)$ where m denotes the evanescent diffraction order that generates the resonance and v marks the corresponding classic waveguide mode. Figure 5(f) shows zero-order reflectance for the case of n=3.5. Under guided-mode lattice resonance in Figs. 5(e) and 5(f), we see that $R_0=1$ for both polarization states at the respective resonance wavelengths. In his example, with a period chosen arbitrarily, there is no correlation between the Mie resonance wavelengths and the GMR wavelengths. This is because there is no causal relationship between the condition $R_0=1$ and Mie resonance.

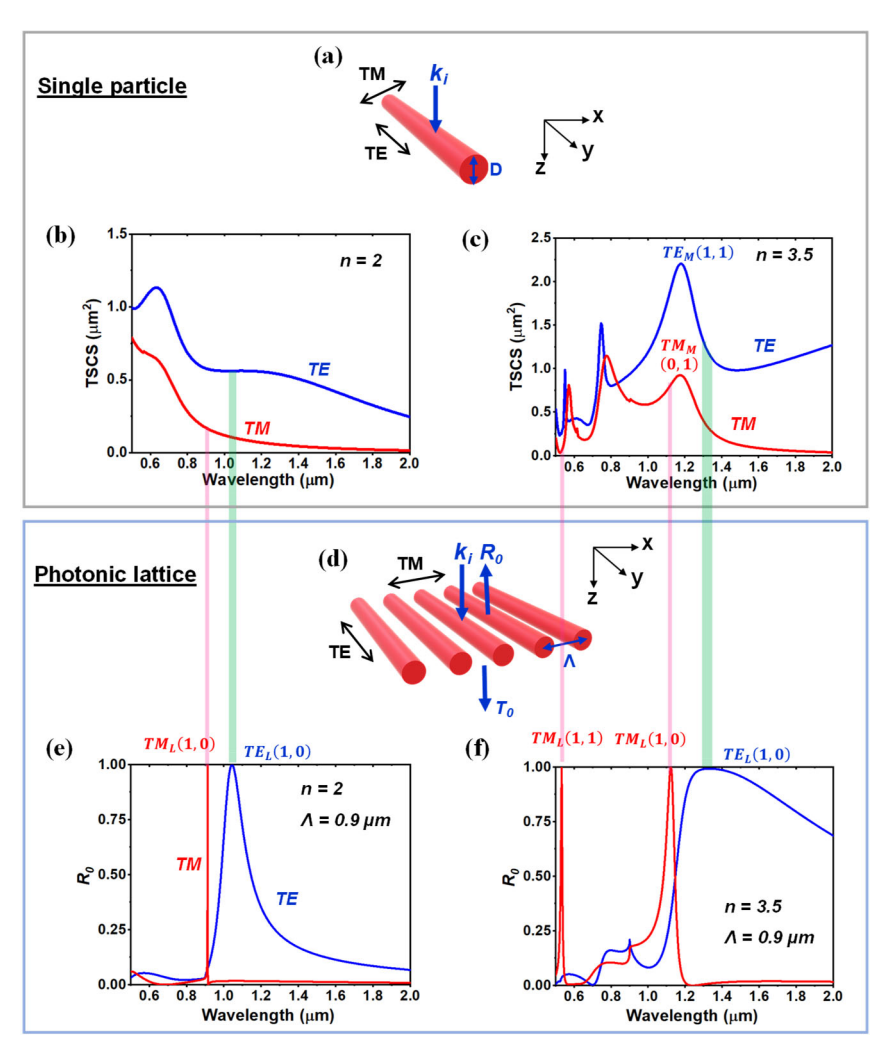


Figure 5. Comparison of single-particle resonance and lattice-resonance spectra. (a), The particle chosen is an infinite circular cylinder with diameter D and refractive index n placed in air. (b) FDTD-computed TSCS spectra under TE and TM polarized light with n=2. (c) TSCS spectra for n=3.5 where the Mie resonance peaks are labeled $TE_M(j, l)$ or $TM_M(j, l)$ by the azimuthal mode number j and the radial mode number l. (d) A photonic lattice arrayed by the elemental cylinder in a. With a representative period (Λ), the zeroth-order reflectance (R_0) spectra are calculated by RCWA. (e) R_0 spectra under TE and TM polarization for n=2. The resonance peaks are labeled $TE_L(m, \nu)$ or $TM_L(m, \nu)$ where m denotes the evanescent diffraction order and ν the waveguide mode. (f) R_0 spectra for n=3.5. We see that there is no correlation between the Mie resonance peaks and the lattice resonance peaks [23].

5. MIE MODAL MEMORY: MATCHED PARTICLE AND LATTICE FIELD PROFILES

At certain spectral locations there is strong correlation with the individual-particle resonance wavelengths and the lattice-resonance wavelengths. We explain this physical manifestation by spatial field matching between the Mie modes and the lateral modes generating the resonance. As the individual cylinders possess characteristic Mie resonance field profiles at the Mie resonance wavelengths, the lateral Bloch modes must match those, at least approximately, at these specific spectral (λ, Λ) coordinates.

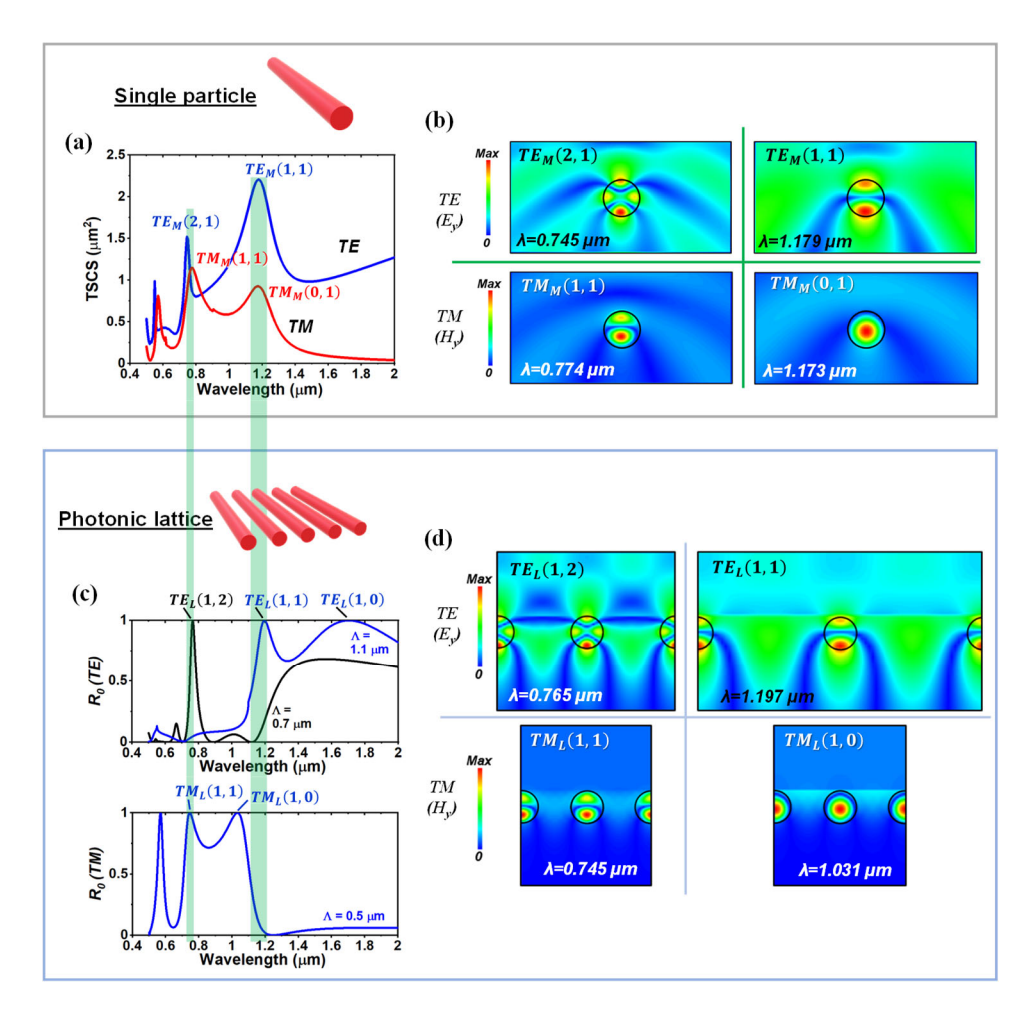


Figure 6. Quantification of local/lateral mode matching. We model a single circular cylinder with D=250 nm and n=3.5 and a corresponding lattice. (a) Total scattering cross section (TSCS) spectra in TE and TM polarized light. Mie resonance peaks are labeled TE_M(j, l) or TM_M(j, l) by azimuthal mode number (j) and radial mode number (l). (b) Electric and magnetic field profiles at Mie resonance wavelengths corresponding to a. E and H indicate the amplitudes of electric and magnetic fields. (c) Photonic lattice spectra $R_0(\lambda)$ at values of Λ chosen to match overlapping Mie/lattice resonance locations. The guided-mode resonance peaks are labeled as TE_L(m, v) or TM_L(m, v) with m denoting the diffraction order and v the waveguide mode. (d) E and H profiles at lattice resonance points corresponding to (c). Comparing (b) and (c) verifies the local/lateral mode matching at these (λ , Λ) coordinates [23].

To verify this idea, we compare TSCS (λ) and $R_0(\lambda)$ spectra and attendant field profiles at values of Λ chosen to match overlapping Mie/lattice resonance locations. In Fig. 6(a), Mie modes $TE_M(1, 1)$ and $TM_M(0, 1)$ occur at $\lambda = 1.179$ µm and 1.173 µm. At higher energy states, $TE_M(2, 1)$ and $TM_M(1, 1)$ are found at $\lambda = 0.745$ µm and 0.774 µm. With periods chosen for resonance coincidence to the extent possible, $R_0(\lambda)$ lattice spectra are displayed in Fig. 6(c) and compared to the Mie resonance wavelengths in Fig. 6(a) with vertical lines. For $\Lambda = 1.1$ µm, the $TE_L(1, 1)$ locates near $TE_M(1, 1)$ and $TE_L(1, 2)$ is closely matched to $TE_M(2, 1)$ at $\Lambda = 0.7$ µm. Similarly, $TM_L(1, 1)$ is close to $TM_M(1, 1)$ at $\Lambda = 0.5$ µm. We now compare

the localized field structures in the cylindrical single particles in Fig. 6(b) with the fields residing in the photonic lattice in Fig. 6(d). We see that the resonant-lattice field patterns approximate the single-particle fields with good qualitative agreement. This is in spite of the fact that the guided-mode resonance wavelengths differ somewhat from the exact Mie resonance wavelengths as quantified in Figs. 6(b) and 6(d). This wavelength difference is reasonable because of the geometric difference of the two physical arrangements. In the lattice, at resonance, there are contradirectional leaky Bloch modes interacting with the particles in addition to the incident wave in stark contrast with the single-particle case. The evanescent-wave-excited lateral modes interacting with the incident wave generate the perfect reflection with the approximate mode matching shown. We conjecture that the mode-matching principle is general and will apply to any dielectric resonant optical lattice independent of the shape of the building block particles constituting the array.

6. CONCLUSIONS

In conclusion, we focus here on the fundamental physical properties of resonant photonic lattices. Summarizing the classic diffractive optics view, we recall that the propagation directions external to periodic lattices are set by the period independent of grating profile. Analogously, the spectral map of perfect reflection is strongly influenced by the period. Classic diffractive effects lie at the heart of these devices, and it is the assembly of particles composing a periodic lattice, as opposed to the individual particle resonance, that yields all main properties. We emphasize that neither local particle-based Fabry-Perot nor Mie resonance is causative in the perfect reflection, or in any other key effects, observed [29-33]. At particular values of period, the particle/lattice fields can match with a corresponding agreement in the resonance wavelength; we refer to this condition as Mie modal memory. The results of this study have potential to advance the field of nanophotonics, including studies of diffractive optics, photonic crystal slabs, metamaterials, metasurfaces, etc., by solidifying the understanding of the physical basis of resonant photonic lattices.

ACKNOWLEDGEMENTS

This research was supported, in part, by the UT System Texas Nanoelectronics Research Superiority Award funded by the State of Texas Emerging Technology Fund as well as by the Texas Instruments Distinguished University Chair in Nanoelectronics endowment. Additional support was provided by the National Science Foundation under Awards No. ECCS-1606898, ECCS-1809143, and IIP-1826966.

REFERENCES

- [1] P. Vincent and M. Neviere, "Corrugated dielectric waveguides: a numerical study of the second-order stop bands," Appl. Phys. 20, 345-351 (1979).
- [2] E. Popov, L. Mashev, and D. Maystre, "Theoretical study of the anomalies of coated dielectric gratings," Optica Acta 33, 607-619 (1986).
- [3] I. A. Avrutsky and V. A. Sychugov, "Reflection of a beam of finite size from a corrugated waveguide," J. Mod. Opt. 36, 1527-1539 (1989).
- [4] G. A. Golubenko, A. S. Svakhin, V. A. Sychugov, and A. V. Tishchenko, "Total reflection of light from a corrugated surface of a dielectric waveguide," Sov. J. Quantum Electron. 15, 886-887 (1985)
- [5] H. Kikuta, H. Toyota, and W. Yu, "Optical elements with subwavelength structured surfaces," Opt. Rev. 10, 63-73 (2003).
- [6] S. Wang and R. Magnusson, "Theory and applications of guided-mode resonance filters," Appl. Opt., 32, 2606-2613 (1993).
- [7] Y. Ding and R. Magnusson, "Resonant leaky-mode spectral-band engineering and device applications," Opt. Express 12, 5661-5674 (2004).
- [8] R. Magnusson and S. S. Wang, "New principle for optical filters," Appl. Phys. Lett. 61(9), 1022-1024 (1992).
- [9] W. Suh and S. Fan, "All-pass transmission or flattop reflection filters using a single photonic crystal slab," Appl. Phys. Lett. 84, 4905-4907 (2004).
- [10] R. F. Kazarinov and C. H. Henry, "Second-order distributed feedback lasers with mode selection provided by first-order radiation losses," IEEE J. Quantum Electron. QE-21, 144-150 (1985).

- [11] D. Rosenblatt, A. Sharon, and A. A. Friesem, "Resonant grating waveguide structures," IEEE J. Quantum Electron. 33, 2038-2059 (1997).
- [12] T. Tamir and S. Zhang, "Resonant scattering by multilayered dielectric gratings," J. Opt. Soc. Am. A 14, 1607-1616 (1997).
- [13] Y. Ding and R. Magnusson, "Band gaps and leaky-wave effects in resonant photonic-crystal waveguides," Opt. Express 15, 680-694 (2007).
- [14] D. Gerace and L. C. Andreani, "Gap maps and intrinsic diffraction losses in one-dimensional photonic crystal slabs," Phys. Rev. E 69, 056603 (2004).
- [15] S. T. Thurman and G. M. Morris, "Controlling the spectral response in guided-mode resonance filter design," Appl. Opt. 42, 3225-3223 (2003).
- [16] H. Wu, J. Hou, W. Mo, D. Gao, and Z. Zhou, "A broadband reflector using a multilayered grating structure with multi-subpart profile," Appl. Phys. B 99, 519–524 (2010).
- [17] S. Peng and G. M. Morris, "Resonant scattering from two-dimensional gratings," J. Opt. Soc. Am. A 13, 993-1005 (1996).
- [18] P. Lalanne, J. P. Hugonin, and P. Chavel, "Optical properties of deep lamellar gratings: a coupled Bloch-mode insight," J. Lightwave Technol. 24, 2442–2449 (2006).
- [19] R. Magnusson, "Wideband reflectors with zero-contrast gratings," Opt. Lett. 39, 4337-4340 (2014).
- [20] C. F. R. Mateus, M. C. Y. Huang, Y. Deng, A. R. Neureuther, and C. J. Chang-Hasnain, "Ultrabroadband mirror using low-index cladded subwavelength grating," IEEE Photon. Technol. Lett. 16, 518–520 (2004).
- [21] N. Gupta and M. S. Mirotznik, "Performance Characterization of tunable longwave infrared filters using quantum cascade laser," Opt. Eng. 57, 127101 (2018).
- [22] G. Mie, "Beiträge zur Optik trüber Medien, speziell kolloidaler Metallösungen," Ann. Phys. 330, 377–445 (1908).
- [23] Yeong Hwan Ko, Nasrin Razmjooei, Hafez Hemmati, and Robert Magnusson, "Perfectly-reflecting guided-mode-resonant photonic lattices possessing Mie modal memory," Opt. Express 29, 26971-26982 (2021).
- [24] Nasrin Razmjooei, Yeong Hwan Ko, Fairooz Abdullah Simlan, and Robert Magnusson, "Resonant reflection by microsphere arrays with AR-quenched Mie scattering," Opt. Express 29, 19183-19192 (2021).
- [25] H. C. van de Hulst, Light Scattering by Small Particles (Wiley, New York, 1957).
- [26] M. G. Moharam and T. K. Gaylord, "Rigorous coupled-wave analysis of planar-grating diffraction," J. Opt. Soc. Am. 71, 811-818 (1981).
- [27] T. K. Gaylord and M. G. Moharam, "Analysis and applications of optical diffraction by gratings," Proc. IEEE 73, 894 (1985).
- [28] L. Cao, J. S. White, J. S. Park, J. A. Schuller, B. M. Clemens and M. L. Brongersma, "Engineering light absorption in semiconductor nanowire devices," Nature Materials 8, 643-647 (2009).
- [29] P. Qiao, W. Yang, and C. J. Chang-Hasnain, "Recent advances in high-contrast metastructures, metasurfaces, and photonic crystals," Adv. Opt. Photon. 10, 180-245 (2018).
- [30] Y. Huang, H. Xu, Y. Lu, and Y. Chen, "All-dielectric metasurface for achieving perfect reflection at visible wavelengths," J. Phys. Chem. C 122, 2990–2996 (2018).
- [31] A. I. Kuznetsov, A. E. Miroshnichenko, M. L. Brongersma, Y. S. Kivshar, and B. Luk'yanchuk, "Optically resonant dielectric nanostructures, "Science 354, aag2472 (2016).
- [32] C. Park, I. Koirala, S. Gao, V. R. Shrestha, S.-Shin Lee, and D. Yong Choi, "Structural color filters based on an all-dielectric metasurface exploiting silicon-rich silicon nitride nanodisks," Opt. Express 27, 667-679 (2019).
- [33] P. Moritra, B. A. Slovick, Z. G. Yu, S. Krishnamurthy, and J. Valentine, "Experimental demonstration of a broadband all-dielectric metamaterial perfect reflector," Appl. Phys. Lett. 104, 171102 (2014).